INSTITUTE OF PHYSICS PUBLISHING PLASMA PHYSICS AND CONTROLLED FUSION

Plasma Phys. Control. Fusion **43** (2001) 1311–1324 PII: S0741-3335(01)23894-9

Neoclassical transport in the CHS device and its outlook for improvement

M F Heyn[1], M Isobe[2], S V Kasilov[3], W Kernbichler[1], K Matsuoka[2], V V Nemov[3], S Okamura[2] and O S Pavlichenko[3]

[1] Institut für Theoretische Physik, Technische Universität Graz, Petersgasse 16, A-8010 Graz, Austria
[2] National Institute for Fusion Science, Oroshi-Chyo 322-6, Toki-city, 509-5292, Japan
[3] Institute of Plasma Physics, National Science Center, 'Kharkov Institute of Physics and Technology', Akademicheskaya Street 1, 61108 Kharkov, Ukraine

Received 12 April 2001
Published 12 September 2001
Online at stacks.iop.org/PPCF/43/1311

Abstract

The $1/\nu$ neoclassical transport is computed for the standard, the drift-orbit-optimized and the quasi-axisymmetric versions of CHS. For the computations, a new method is used which is based on the integration along magnetic field lines. The calculations show the advantage of the quasi-axisymmetric CHS configuration over the standard configuration resulting in a reduced $1/\nu$ transport. It is shown that also for the drift-orbit-optimized configuration the $1/\nu$ transport is reduced; however, by a smaller amount than for the quasi-axisymmetric configuration.

1. Introduction

The investigations on CHS are an important part of the World stellarator programme. The CHS heliotron/torsatron represents those present stellarator devices with a helical winding and with compensating coils. A series of experiments on plasma confinement have been carried out on this device [1–3, 5]. At the same time, a number of propositions were made to improve the CHS confinement properties [4–6].

Neoclassical transport in the long-mean-free-path regime is one of the most important questions related to the properties of stellarator plasma confinement. Among various transport regimes in stellarators, the so-called $1/\nu$ transport regime is the most unfavorable. Therefore, minimization of neoclassical transport in this regime is one of the key issues in stellarator optimization [7]. On the basis of a new approach developed in [8], in this paper the $1/\nu$ transport properties are computed for three versions of the CHS configuration. This new computational method is based on the integration along magnetic field lines in a given magnetic field. The method is valid for any stellarator magnetic field and allows for a completely uniform treatment in any kind of quasi-symmetry. Beside this, for vacuum configurations all magnetic fields can

be derived from realistic coil models. In the present work, the magnetic field strength is computed using the Biot–Savart law.

First, the standard CHS configuration [1–3, 5] is analysed. In addition, the drift-orbit-optimized configuration [4, 5] which is very close to an omnigenious configuration is studied. Note that the drift-orbit-optimized CHS configuration is an inward shifted configuration and that its properties are rather close to those for 'sigma optimization', which has already been analysed for approximate analytic field representations (see, e.g., [9–11]). Finally, the quasi-axisymmetric version of CHS (CHS-qa) [6] is analysed. To analyse the underlying $1/\nu$ transport properties of particle drift motion in these configurations and to view the tendencies of transport properties in the presence of an electric field, the bounce averaged trapped particle drift velocity across magnetic surfaces is also computed and discussed.

From these results it follows that the strongest reduction in the $1/\nu$ transport takes place for the quasi-axisymmetric CHS-qa configuration. It is also shown that the drift-orbit-optimized version of CHS has some less pronounced advantage over the standard configuration. In general, the result for the CHS-qa configuration looks very attractive. However, it should be noted that this computation is carried out for a vacuum magnetic field. Therefore, this very attractive result must be confirmed for CHS-qa for the case of finite beta. The corresponding study is planed to be performed in the future.

2. Initial points

The magnetic field of the low-aspect-ratio CHS device has a rich spectrum of helical and mirror-like harmonics and some kind of multi-helicity approach has to be used for low-collisionality transport calculations. At present, a number of analytical and numerical approaches are used to address this question. In the method used here, the neoclassical transport coefficients in the $1/\nu$ regime are calculated by integration along magnetic field lines [8]. Such an integration takes into account particles being trapped within one magnetic field ripple as well as particles being trapped within several magnetic field ripples. One of the advantages of this method is the fact that, for a magnetic field available in real-space coordinates, calculations can be performed without a field transformation to magnetic coordinates. In accordance with [8], the energy flux density averaged over a magnetic surface can be presented in the form

$$F_T = -\frac{\sqrt{8}}{9\pi^{3/2}}\frac{v_T^2\rho_{\mathrm{L}}^2}{\nu R^2}\epsilon_{\mathrm{eff}}^{3/2}\int_0^\infty \frac{\mathrm{d}z\,\mathrm{e}^{-z}z^{7/2}}{A(z)}\frac{nT}{f_0}\frac{\partial f_0}{\partial r} \tag{1}$$

$$\epsilon_{\mathrm{eff}}^{3/2} = \frac{\pi R^2}{8\sqrt{2}}\lim_{L_s\to\infty}\left(\int_0^{L_s}\frac{\mathrm{d}s}{B}\right)\left(\int_0^{L_s}\frac{\mathrm{d}s}{B}|\nabla\psi|\right)^{-2}\int_{B_{\min}^{(\mathrm{abs})}/B_0}^{B_{\max}^{(\mathrm{abs})}/B_0}\mathrm{d}b'\sum_{j=1}^{j_{\max}}\frac{\hat{H}_j^2}{\hat{I}_j} \tag{2}$$

$$\hat{H}_j = \frac{1}{b'}\int_{s_j^{(\min)}}^{s_j^{(\max)}}\frac{\mathrm{d}s}{B}\sqrt{b'-\frac{B}{B_0}}\left(4\frac{B_0}{B}-\frac{1}{b'}\right)|\nabla\psi|k_G \qquad \hat{I}_j = \int_{s_j^{(\min)}}^{s_j^{(\max)}}\frac{\mathrm{d}s}{B}\sqrt{1-\frac{B}{B_0b'}}. \tag{3}$$

Here $f_0 = f_0(\psi, w)$ is the Maxwellian distribution as a function of the particle energy w and the magnetic surfaces, labelled ψ; $v_T = \sqrt{2T/m}$ is the thermal velocity; $\rho_{\mathrm{L}} = mcv_T/(eB_0)$ is the mean Larmor radius; B_0 is a reference magnetic field, $\nu A(z)$ is a pitch-angle scattering frequency [12], R is the major radius of the torus; $\partial f_0/\partial r$ is the average normal derivative; and $k_G = (\boldsymbol{h}\times(\boldsymbol{h}\cdot\nabla)\boldsymbol{h})\cdot\nabla\psi/|\nabla\psi|$ is the geodesic curvature of a magnetic field line with the unit vector $\boldsymbol{h} = \boldsymbol{B}/B$.

The integral over $z = mv^2/(2T)$ in (1) corresponds to the integration over the particle energy w. The characteristic features of the specific magnetic field geometry manifest

themselves through the factor $\epsilon_{\rm eff}^{3/2}$, where $\epsilon_{\rm eff}$ is the so-called effective ripple. This factor naturally takes into account contributions to the $1/\nu$ transport arising from all classes of trapped particles. Here a class of particles is defined by the number of local magnetic field minima within the respective trapping region.

The quantity $\epsilon_{\rm eff}$ is calculated by integration over the magnetic field line length, s, over the sufficiently large interval 0–L_s, and by integration over the perpendicular adiabatic invariant of trapped particles, $J_\perp$, by means of the variable b'. Here, $B_{\rm min}^{\rm (abs)}$ and $B_{\rm max}^{\rm (abs)}$ are the minimum and maximum values of B within the interval 0–L_s. The quantities $s_j^{\rm (min)}$ and $s_j^{\rm (max)}$ within the sum over j in (2) correspond to the turning points of trapped particles. These quantities are found during the integration along the magnetic field line by tracing the sign changes of the expression under the square root in (3). The result (1) differs from the corresponding formula for the classical stellarator model [12], by a simple replacement of the helical ripple along the magnetic field line, $\epsilon_{\rm h}$, with the quantity $\epsilon_{\rm eff}$. Therefore, for any magnetic configuration the $1/\nu$ transport coefficients can be obtained from the corresponding coefficients for the classical stellarator model with the replacement of $\epsilon_{\rm h}$ by $\epsilon_{\rm eff}$.

The computation of (2) and (3) is performed by integration along a magnetic field line placed on the magnetic surface under consideration. Therefore, these equations must be supplemented by the differential equations of the magnetic field line. For calculation of $\nabla\psi$, which enters into (2) and (3) directly as well as through k_G, the corresponding equations are also used which allow one to find $\nabla\psi$ using integration along the magnetic field line (see [8]).

To apply formulae (1) and (2) to study the transport in specific configurations, the magnetic field and its spatial derivatives must be calculated for these configurations. The toroidal and helical magnetic fields for the standard [1–3] and the drift-orbit-optimized [4, 5] configurations of CHS are produced by a helical winding current. This is computed using the Biot–Savart law for the helical conductor modelled with eight filaments in three layers, where the layers contain two, three and three filaments, respectively. The layers are counted from the inner side of the conductor. The distribution of the filaments is roughly uniform within the conductor cross section.

For CHS-qa [6] the magnetic field is produced by modular coil currents in 20 coils. The number of the magnetic field periods along the torus is two, and the aspect ratio is 3.9. Each of these coils is modelled by a closed filamentary conductor and the magnetic field is again calculated with the use of the Biot–Savart law.

3. Computational results for the effective ripple

The integration along the field line is performed over the interval 0–L_s, where L_s corresponds to 250 magnetic field periods. The calculations are performed in cylindrical coordinates, ρ, φ and z.

Figures 1–3 show the magnetic surfaces which are used for $\epsilon_{\rm eff}^{3/2}$ computations for the standard CHS configuration ($R_{ax} = 92.1$ cm), for the drift-orbit-optimized configuration ($R_{ax} = 87.7$ cm) and for the CHS-qa configuration. The quantity R_{ax} indicates the position of the magnetic axis in the $\varphi = 0$ plane. The cross sections for $\varphi = 0$ and for $\varphi = \pi/n_p$ (one-half of the magnetic field period) are presented, where n_p is the number of magnetic field periods. In figure 4, the rotational transforms are shown for all three configurations. The magnetic surfaces are characterized by the starting point of the integration, $\rho = R_{\rm st}$, at $\varphi = 0$ and $z = 0$. Some of the $R_{\rm st}$ values are shown in figure captions. Note that small islands for the rotational transform $\iota = 1$ are not shown in figure 1 and that the island surface in figure 2 corresponds to $\iota = 4/5$.

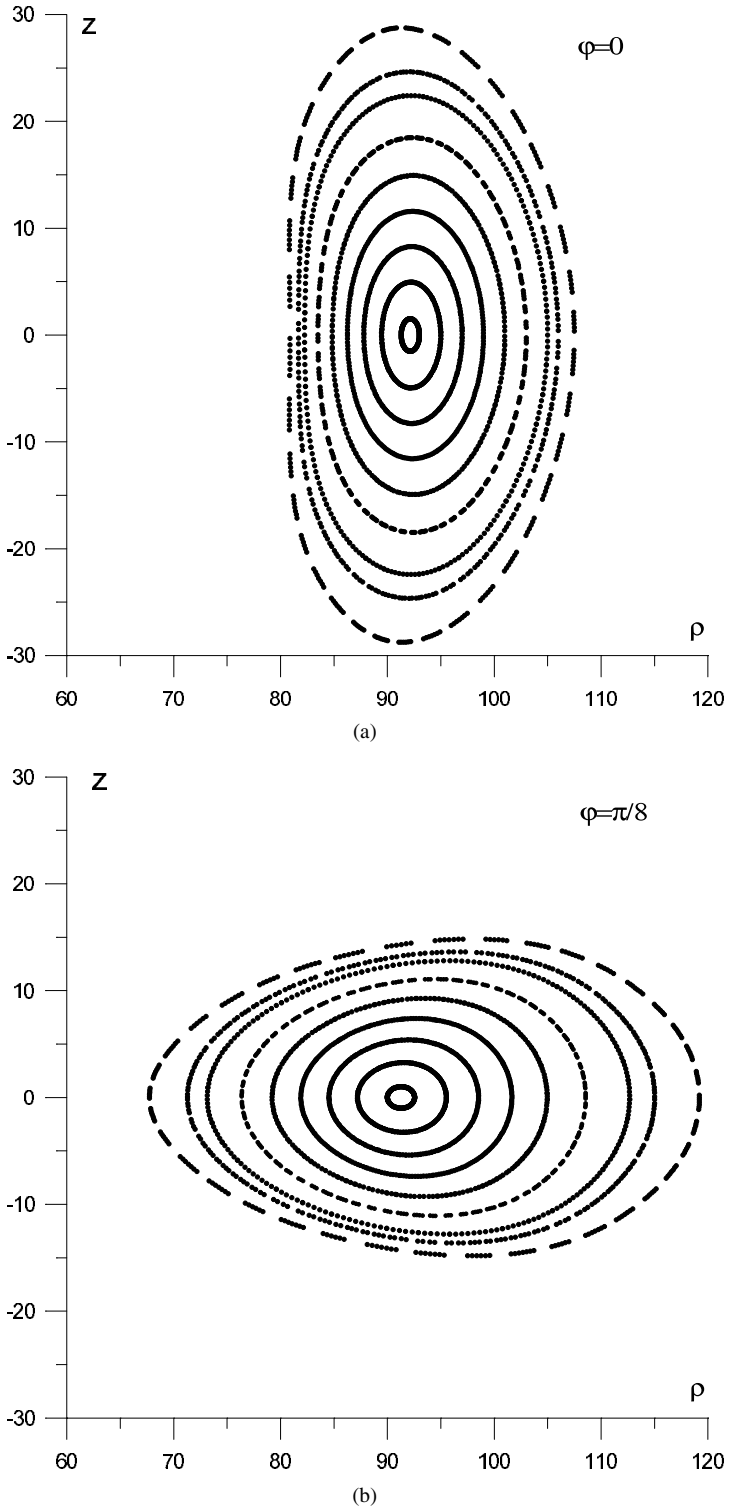

Figure 1. Standard configuration of CHS ($R_{ax} = 0.921$ m); the magnetic surfaces at the toroidal cross sections are $\varphi = 0$ and $\varphi = \pi/8$, respectively (the dimensions are in centimetres).

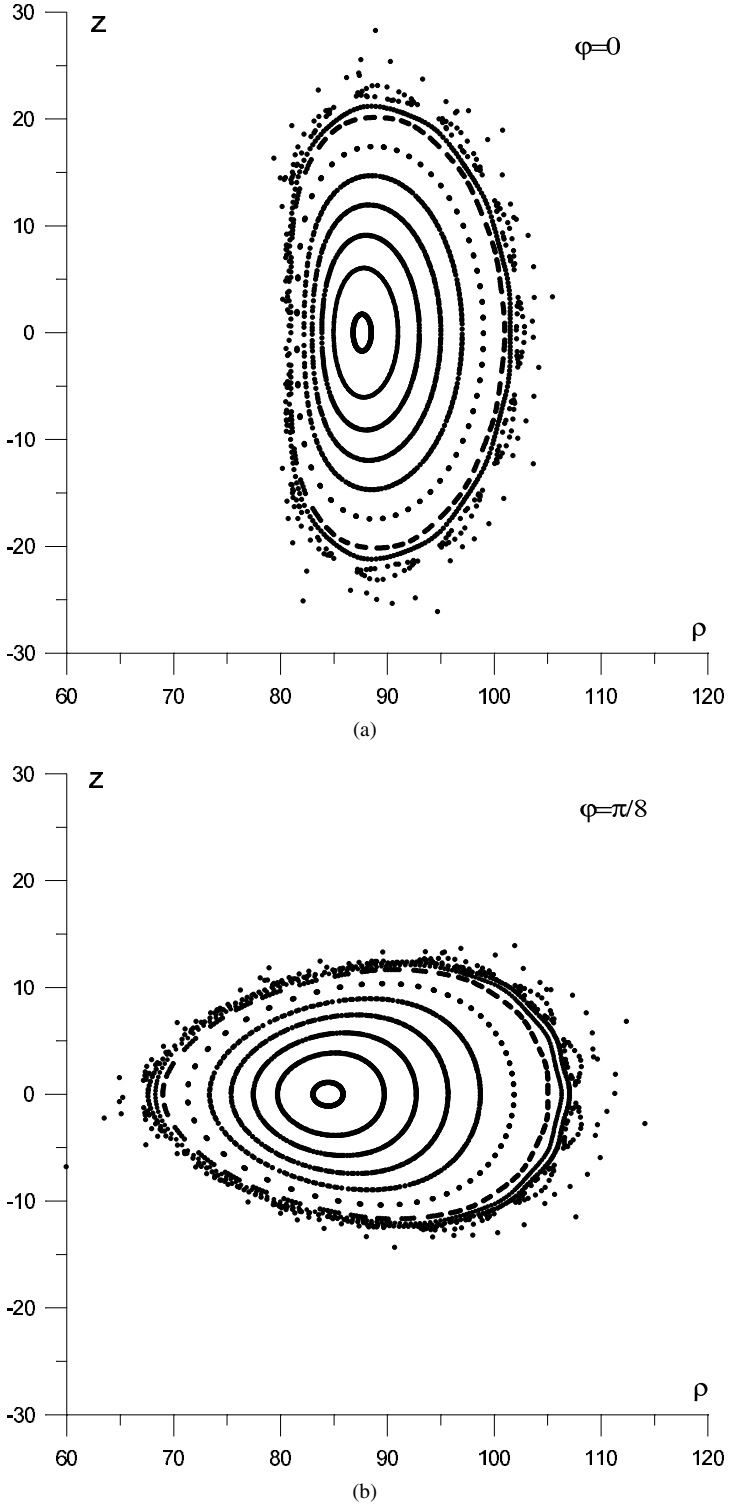

Figure 2. Drift-orbit-optimized configuration of CHS ($R_{ax} = 0.877$ m); the magnetic surfaces at the toroidal cross sections are $\varphi = 0$ and $\varphi = \pi/8$, respectively (the dimensions are in centimetres).

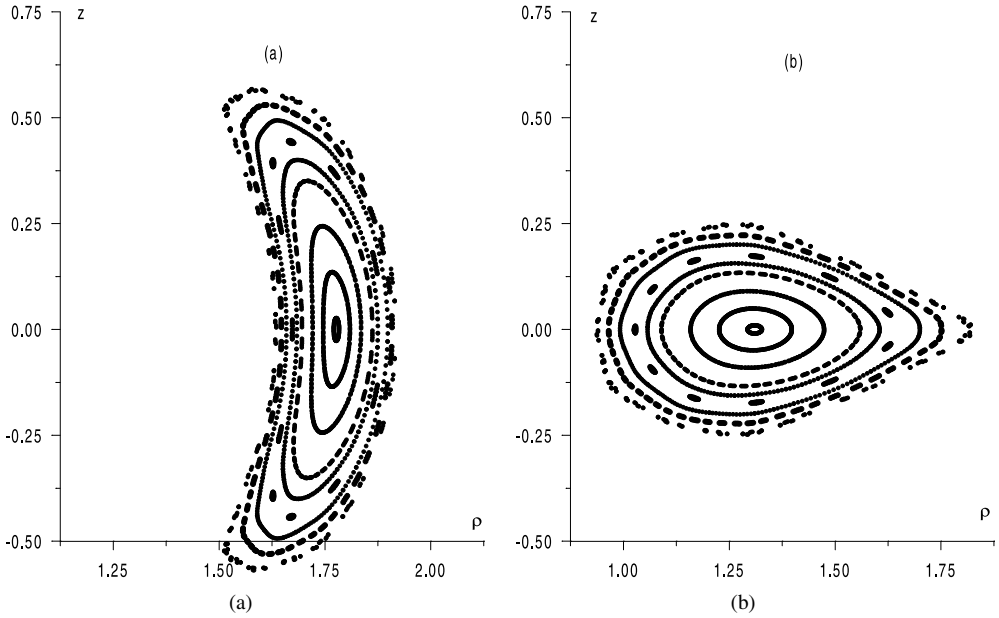

Figure 3. Magnetic surfaces for CHS-qa for $R_{\rm st} = 1.771, 1.746, 1.721, 1.696, 1.684, 1.672$ (island surface), 1.659, 1.647 and 1.635 (island surface): (a) $\varphi = 0$ and (b) $\varphi = \pi/2$ (the dimensions are in metres).

The results of the $\epsilon_{\rm eff}^{3/2}$ computations are shown in figure 5. From the modulation of B along the magnetic field line, the quantity ϵ_h can be found. Using this quantity, one can find that for the the standard configuration of CHS at moderate distances from the magnetic axis, the $\epsilon_{\rm eff}^{3/2}$ value is somewhat greater (by a factor of up to two) than that for a classical stellarator with the same aspect ratio.

For the drift-orbit-optimized configuration, the $\epsilon_{\rm eff}^{3/2}$ value turns out to be approximately a factor of 10 smaller than the value for the standard configuration. As pointed out in [4, 5], this configuration is very close to the omnigenious configuration and, therefore, has improved confinement of locally trapped particles. The results give a quantitative evaluation of such an improvement.

It is seen from figure 5 that for the CHS-qa configuration, the value of $\epsilon_{\rm eff}^{3/2}$ is reduced much more. For almost all values of r/R, $\epsilon_{\rm eff}^{3/2}$ is two to three orders of magnitude smaller as compared to those for the standard configuration of CHS. The $\epsilon_{\rm eff}^{3/2}$ value increases towards the boundary and towards the centre of the configuration. A minimum $\epsilon_{\rm eff}^{3/2}$ value is reached at $r/R \approx 0.08$. A sharp increase in $\epsilon_{\rm eff}^{3/2}$ is seen for the island magnetic surface corresponding to $r/R \approx 0.15$ with $R_{\rm st} = 1.672$. Such an increase shows that inside the magnetic islands local magnetic configurations are formed for which the confinement properties can differ from those for the basic non-island magnetic surfaces. Over the whole radius, the values of $\epsilon_{\rm eff}^{3/2}$ for CHS-qa are close to those for the quasi-helically symmetric (QHS) configuration [8] which is a real-space realization of the original quasi-helically symmetric stellarator [13]. However, this is true for an even wider range of r/R than in QHS.

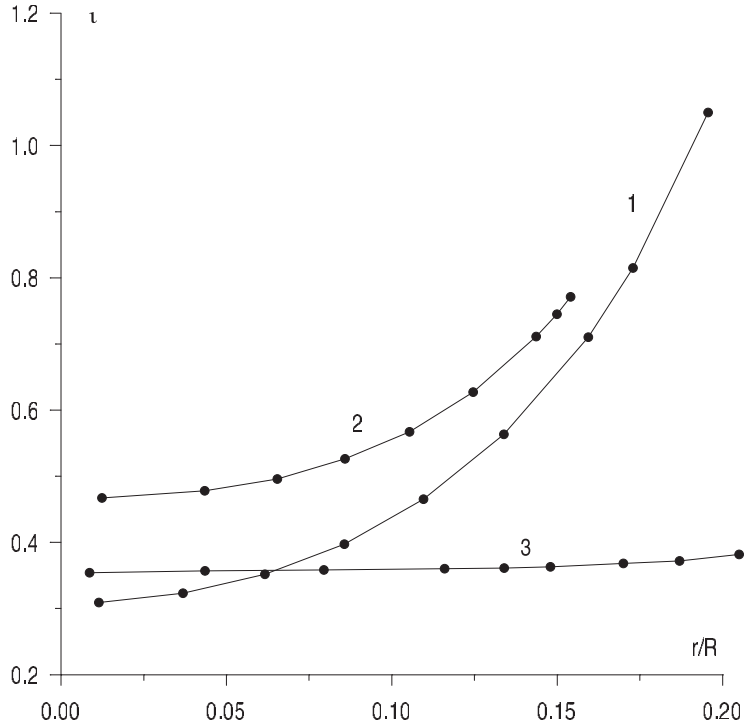

Figure 4. Rotational transform (in units of 2π) for the standard configuration of CHS (curve 1), for the drift-orbit-optimized configuration of CHS (curve 2) and for CHS-qa (curve 3).

4. Bounce-averaged trapped particle drift velocity

It follows from the neoclassical transport theory that the asymmetric long-mean-free-path transport for any regime is directly connected to the trapped particle orbit displacement from the flux surface, Δr, during a bounce period τ_b due to the ∇B drift. Here, r is the formal radius of the magnetic surface. One can define the bounce-averaged trapped particle drift velocity across a magnetic surface as $v_{an} = \Delta r/\tau_b$. From neoclassical theory follows that a decrease in v_{an} leads to a decrease of the asymmetric neoclassical transport in all regimes and that the transport coefficients approximately scale with v_{an}^2 also in all regimes.

In fact, the $\epsilon_{eff}^{3/2}$ quantity considered in the preceding section takes into account a square average of v_{an} that is averaged over the pitch angle with a weight which is specific for the confinement regime. For various transport regimes, different regions of pitch angles are important for neoclassical losses. Therefore, it is of interest to make a direct computation of v_{an} as a function of the pitch angle and of the position on a magnetic surface. Such a computation is presented in this section for some of the magnetic surfaces of the various CHS configurations. The technique presented in [8, 14] is used for this purpose.

The v_{an} quantity was calculated for the local minima of B placed along a magnetic field line. The computational results are presented with the help of normalized quantities. The parameter η is given as a function of γ. The parameter η is a normalized v_{an}, where the normalization is performed in such a way that for the model field of a classical stellarator [12] the maximum η value, η_m, is $\eta_m = 0.5$. The parameter $\gamma = v_{\|i}/v_{\perp 0}$ is directly related to the

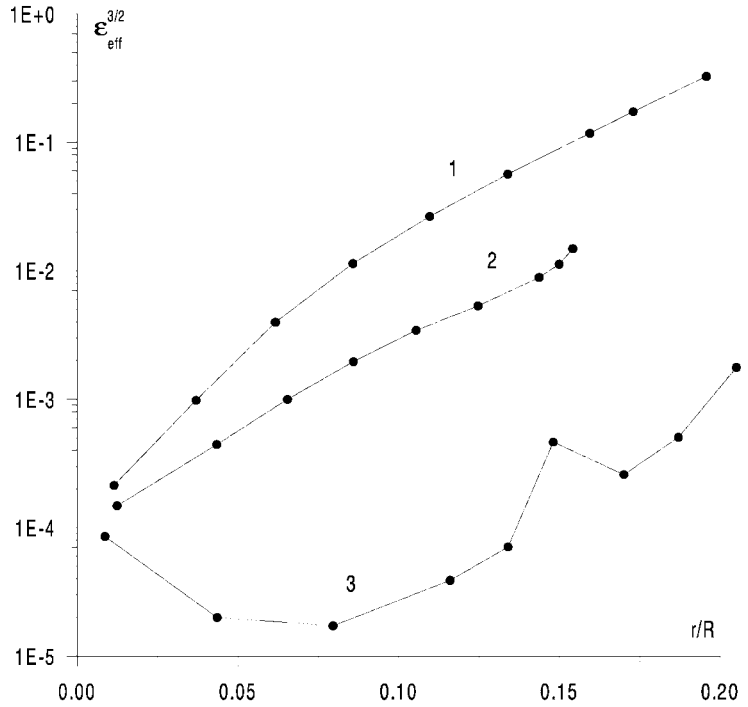

Figure 5. Parameter $\epsilon_{\rm eff}^{3/2}$ for the standard configuration of CHS (curve 1), for the drift-orbit-optimized configuration of CHS (curve 2) and for CHS-qa (curve 3).

depth of particle trapping or, in other words, to the pitch angle at the point of a local minimum of B, $v_{\|i}$ is $v_\|$ at this point, $v_{\perp 0} = \sqrt{J_\perp B_0}$.

Figures 6–8 show the distribution of the magnetic field module, B, along magnetic field lines for those magnetic surfaces for which calculations of η are performed. For the standard and the drift-orbit-optimized CHS configurations the magnetic surfaces correspond to $r/R \approx 0.086$. For a comparison of those configurations, the magnetic surfaces at moderate distances from the magnetic axes are chosen. The magnetic surface corresponding to $r/R \approx 0.18$ ($R_{\rm st} = 1.647$) was chosen for CHS-qa. On this surface one gets the highest $\epsilon_{\rm eff}^{3/2}$ value for any non-island surface. For convenience, some of the local B minima are marked by numbers in the respective figures.

Results for η are presented in figures 9–11, respectively. The curves are numbered in accordance with the numbering of the minima of B. Non-zero values of η are seen for the γ interval $0 \leqslant \gamma \leqslant \gamma_{\rm max}$ which corresponds to pitch angles of trapped particles. The highest η values are seen for those values of γ which correspond to those particles being trapped within a single ripple well. The η values for particles being trapped within a few ripple wells are much smaller. This interval of γ values can be seen to the right of the sharp decrease of η.

For the standard configuration of CHS, the maximum value of η (figure 9) reaches $\eta_{\rm m} \approx 0.55$ and in practice does not depend on γ for the γ interval corresponding to particles being trapped within a single ripple well. This is in a good qualitative agreement with the η dependence for the classical stellarator and with results of the $\epsilon_{\rm eff}^{3/2}$ computation in the preceding section.

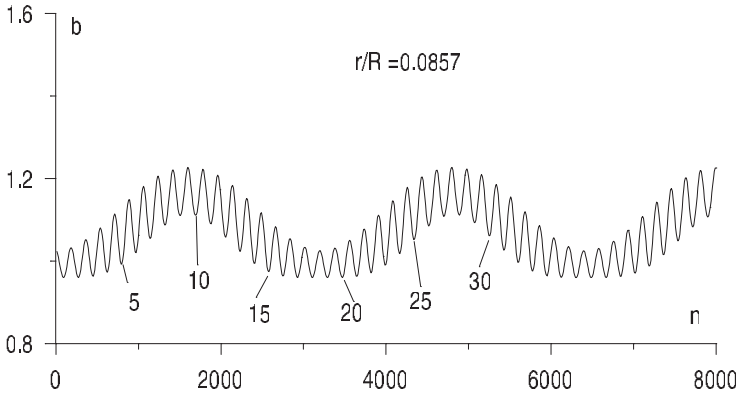

Figure 6. Module of B/B_0 versus number of integration steps along the field line n for the standard configuration of CHS with 160 steps within one magnetic field period. Some of local minima of B are numbered.

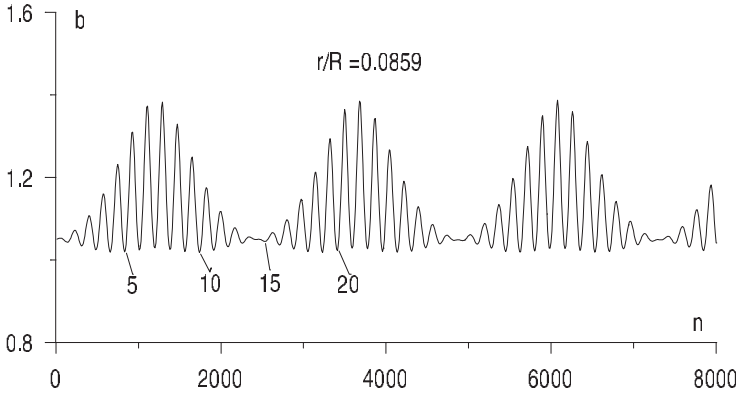

Figure 7. The same as in figure 6 for the drift-orbit-optimized configuration of CHS.

For the drift-orbit-optimized configuration, the η value (figure 10) is rather small for sufficiently small values of γ representing deeply trapped particles. It increases with γ when γ approaches the transition region between different classes of trapped particles. It can be easily seen that overall the η values are smaller than those for the standard configuration of CHS. This correlates with the computational results for $\epsilon_{\rm eff}^{3/2}$ and with the improved confinement within the $1/\nu$ transport regime in the drift-orbit-optimized configuration as compared to the standard CHS configuration.

However, for γ values close to the transition region between particles being trapped within a single ripple well and those being trapped within two or more ripple wells, the η values for the drift-orbit-optimized configuration are close to those for the standard configuration of CHS. Therefore, one should not expect a substantial improvement of the neoclassical transport in the drift-orbit-optimized configuration as compared to the standard stellarator for the so-called $\sqrt{\nu}$ and ν regimes. This is due to the fact that this fraction of helically trapped particles gives the main contribution to the neoclassical transport for those regimes [12]. Note that for these low-collisional regimes and for $\nu/\epsilon_h \leqslant |\omega_E|$, an important role belongs to banana precession around the magnetic axis due to the radial electric field with the poloidal drift frequency ω_E.

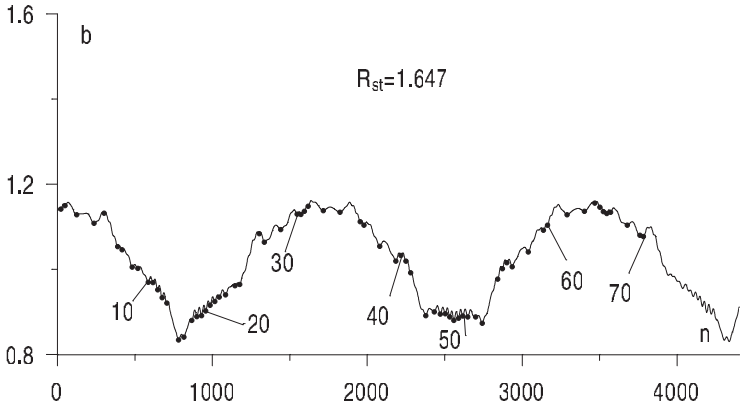

Figure 8. Module of B/B_0 against the number of integration steps along the field line n for CHS-qa with 320 steps for one magnetic field period. Local minima of B are marked and some of them are numbered.

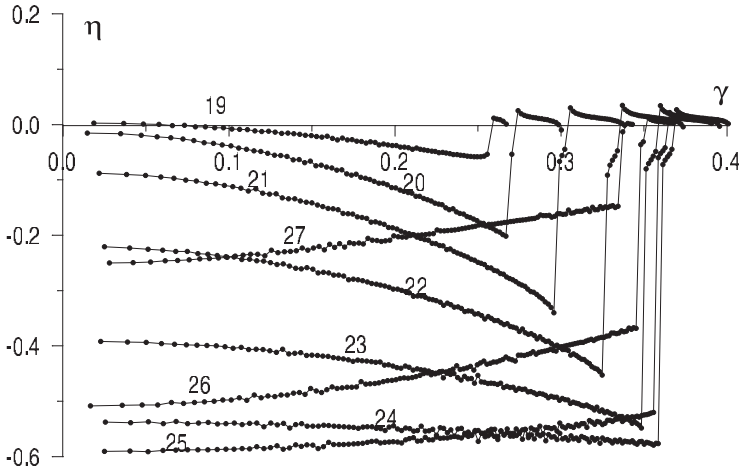

Figure 9. Parameter η as a function of γ for the magnetic surface of the standard configuration of CHS. For the minima of B numbered 18, 17, 16, 15, 14, 13, 12, 11 and 10, the η values are approximately equal in magnitude but opposite in sign to those in the graph numbered 19, 20, 21, 22, 23, 24, 25, 26 and 27, respectively (see figure 6).

In figure 11 the results for CHS-qa are shown. For most curves, only those η values which correspond to particles being trapped within a single ripple well are shown. The rather small η values for larger γ values are omitted. It follows from the calculations that minimum values of η correspond to maximum values of the local minima of B (e.g., curves 30–35 in figure 11). The η_m value is approximately 1.5 times smaller than that for the standard configuration of CHS. The γ limits corresponding to rather high η values are substantially smaller than those for the standard configuration. Both reasons lead to the substantial decrease of the effective ripple which was obtained in the preceding section for CHS-qa. Nevertheless one should bear in mind that there is a small fraction of trapped particles with rather high trapped particle drift velocities where η_m is about two-thirds of η_m for the standard stellarator. Such particles can be lost for sufficiently small collision frequencies.

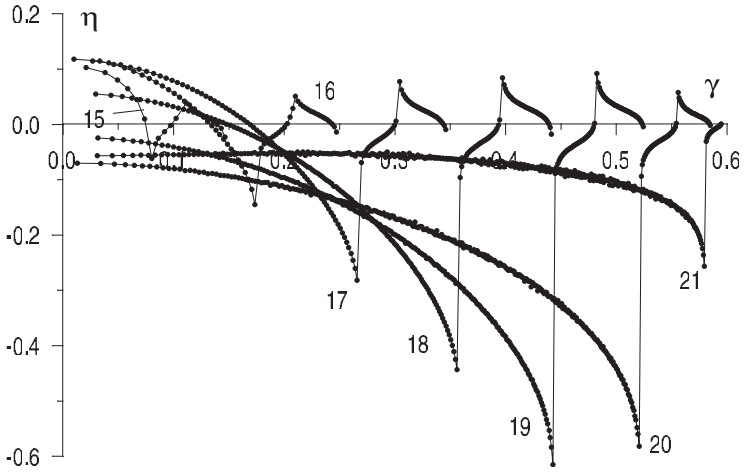

Figure 10. Parameter η as a function of γ for the magnetic surface of the drift-orbit-optimized configuration of CHS. For minima of B numbered 14, 13, 12, 11, 10, 9 and 8 the η values are approximately equal in magnitude but opposite in sign to those in the graph numbered 15, 16, 17, 18, 19, 20 and 21, respectively (see figure 7).

To estimate the upper limit of this characteristic collision frequency, $\nu_{\rm cr}$, in the absence of a radial electric field, one can equate two characteristic times: a time $\tau_{\rm d}$ for particle drift motion across the small plasma radius, a, ($\tau_{\rm d} \approx a/v_{\rm an}$, $v_{\rm an} \approx \eta_{\rm m} v_{\rm dr}$, $v_{\rm dr} \approx \rho_{\rm L} v_T/R$) and a collisional detrapping time of trapped particles. For particles being trapped within a single ripple well, this detrapping time is $\gamma_{\rm 1m}^2/\nu_{\rm cr}$ with γ_{1m} being the upper γ limit for such a particle. As a result, one obtains

$$\nu_{\rm cr} \approx \gamma_{\rm 1m}^2 \eta_{\rm m} v_{\rm dr}/a. \tag{4}$$

For the standard CHS configuration and for CHS-qa, $\gamma_{\rm 1m}$ is approximately 0.4 and 0.1, respectively. Therefore, neglecting the difference in $\eta_{\rm m}$ values, one obtains that for CHS-qa the $\nu_{\rm cr}$ value is approximately 16 times smaller than that for the standard CHS configuration.

Calculations of the parameter η are also performed for the magnetic surface with $r/R \approx 0.08$ ($R_{\rm st} = 1.721$, the minimum $\epsilon_{\rm eff}^{3/2}$ value, see figure 5). For this case, the η dependences on γ turn out to be qualitatively similar to those in figure 11. However, the maximum γ values for locally trapped particles turn out to be in the range 0.05–0.08 and are two to three times smaller than those given in figure 11. This is accompanied by an insignificant decrease of the $\eta_{\rm m}$ values. Such a decrease in γ agrees with the decrease in $\epsilon_{\rm eff}^{3/2}$ by one order of magnitude, which is seen in figure 5 since $\epsilon_{\rm eff}^{3/2}$ is proportional to $\gamma_{\rm max}^3$ if all other conditions are the same.

Discussing the features of the bounce averaged ∇B drift in relation to the general optimization of stellarator neoclassical transport, one can state that (i) the fraction of ripple-trapped particles in CHS-qa is significantly smaller compared to the other two CHS configurations; (ii) the improvement of $1/\nu$ neoclassical transport for the drift-orbit-optimized CHS configuration and the similarity of $\sqrt{\nu}$ transport for the drift-orbit-optimized and the standard CHS configurations correlate with predictions for sigma optimization; (iii) in spite of the avoidance of the ripple-trapped particle majority in regions of strong radial ∇B drift in CHS-qa, there exists some fraction of ripple-trapped particles with a rather large radial drift.

It is of interest to point out the following difference between quasi-axial and quasi-helical symmetries. For the quasi-axial symmetry, the trapped particle drift velocity across a magnetic

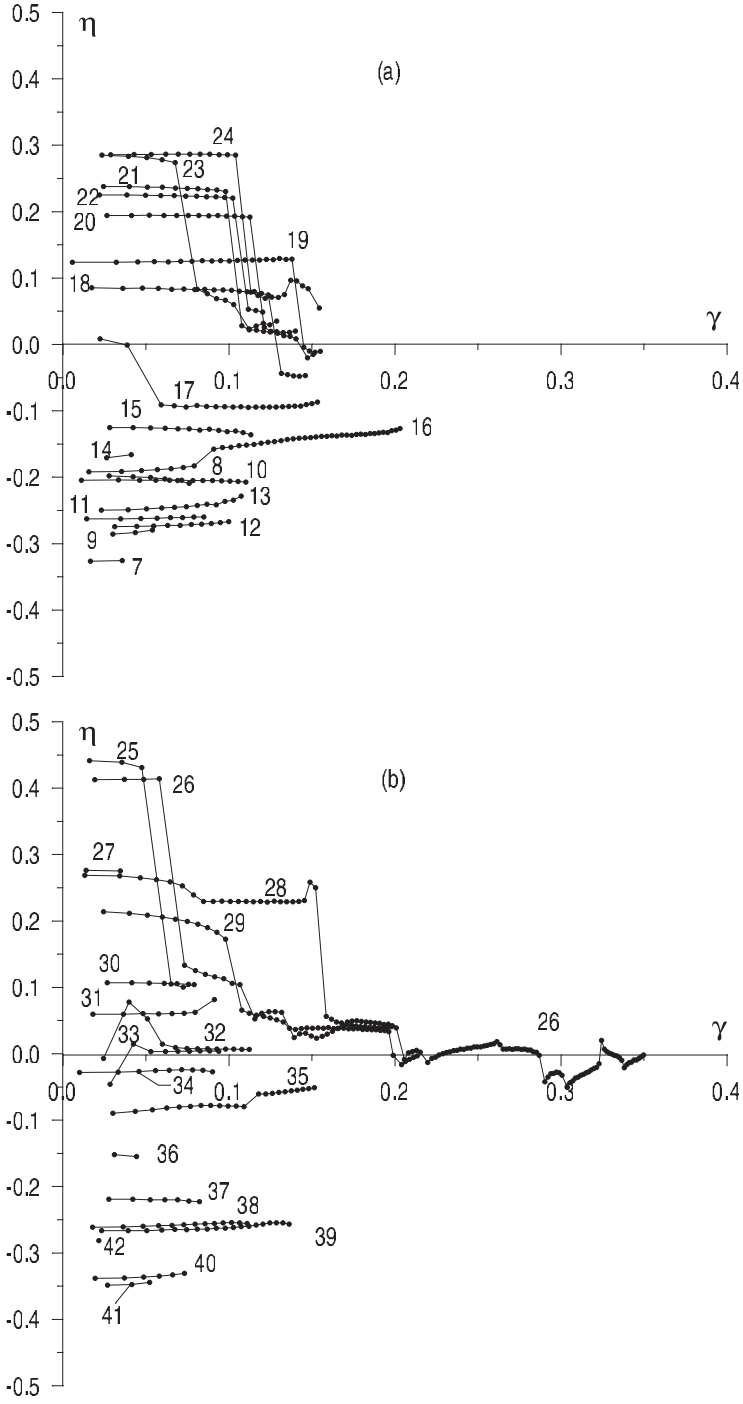

Figure 11. Parameter η as a function of γ for the magnetic surface of CHS-qa at $R_{st} = 1.647$. The curve numbering corresponds to the numbering of B minima in figure 8: (a) minimum B points numbered from 7 to 24, (b) minimum B points numbered from 25 to 42 and (c) minimum B points numbered from 43 to 57.

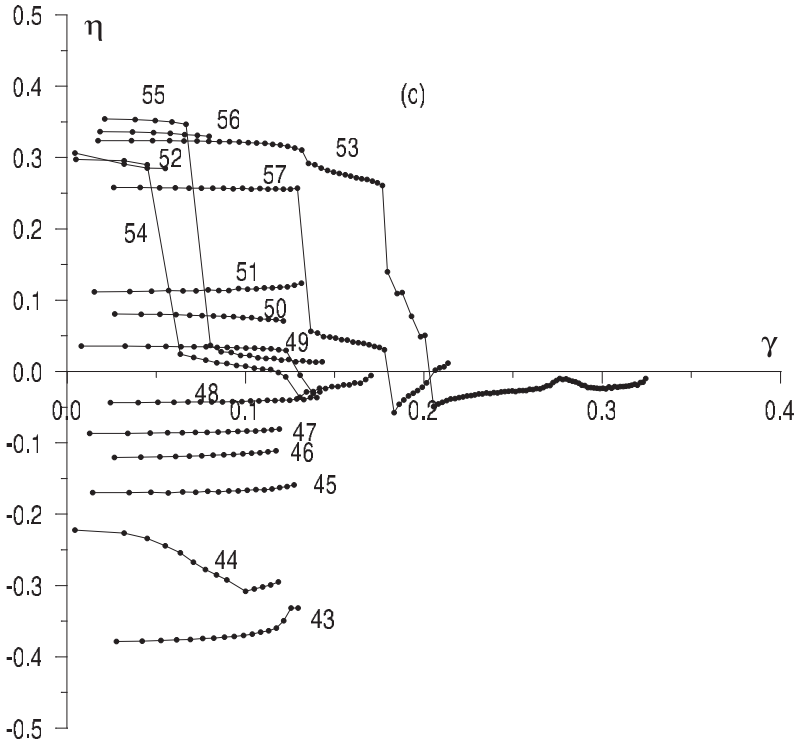

Figure 11. (Continued)

surface, v_{an}, is not reduced very much but the number of locally-trapped particles (trapped within a single ripple well) is strongly reduced. The maximum γ value corresponding to such particles is strongly reduced, see figure 11. At the same time for the quasi-helical symmetry the number of locally-trapped particles is practically not reduced whereas the velocity v_{an} is reduced strongly [14].

5. Conclusions

It follows from the effective ripple calculations that the level of the $1/\nu$ transport for the standard configuration of CHS is somewhat greater than the analogous level for the classical stellarator model. The factor is up to two at intermediate distances from the magnetic axis.

For the drift-orbit-optimized CHS configuration, the level of transport in the $1/\nu$ regime turns out to be approximately a factor of 10 smaller than that for the standard configuration. However, for the $\sqrt{\nu}$ and ν transport regimes a reduction in the transport should not be so substantial. This follows from the calculation of the bounce-averaged trapped particle drift velocity across the magnetic surface, v_{an}.

The strongest reduction in the $1/\nu$ transport takes place for CHS-qa. The level of this transport turns out to be two to three orders of magnitude smaller than that for the standard configuration of CHS. So, the $1/\nu$ transport in CHS-qa turns out to be at the same level as that for a quasi-helically symmetric stellarator. However, for the quasi-helical symmetry the decrease of the $1/\nu$ transport occurs due to the substantial reduction of v_{an}. This is even true for the near boundary region of the magnetic configuration and, therefore, all the trapped particles

are well confined. In contrast, for CHS-qa the transport reduction occurs mainly due to the substantial reduction in the number of locally trapped particles. The maximum ν_{an} value is smaller than that for the classical stellarator model, but the decrease is not very large.

Thus, the neoclassical confinement properties of CHS-qa are substantially better than those for the standard and the drift-orbit-optimized configurations of CHS, respectively; although a small fraction of locally-trapped particles exists, which can be lost when the collision frequency is rather small.

Acknowledgments

This work was partly supported by the Association EURATOM-OEAW, by the Austrian Academy of Sciences and by the 'Monbusho International Scientific Research Program: Joint Research' (Japan).

References

[1] Iiyoshi A 1997 *Fusion Energy* vol 1 (Vienna: IAEA) p 113
[2] Ida K *et al* 1998 *Proc. 17th IAEA Fusion Conf. (Yokohama, 1998)* IAEA-CN-69/EX2/2
[3] Ida K *et al* 1999 *Nucl. Fusion* **39** 1649
[4] Okamura S, Matsuoka K, Kubo S and Idei H 1997 *Annual Report of NIFS (April 1996–March 1997)* p 225
[5] Okamura S *et al* 1999 *Nucl. Fusion* **39** No 9Y 1337
[6] Okamura S *et al* 2000 *Proc. 27th EPS Conf. on Controlled Fusion and Plasma Physics (Budapest, Hungary, 12–16 June, 2000)* ed K Szego, T N Todd and S Zoletnik, Report P4.018
[7] Grieger G *et al* 1992 *Phys. Fluids* B **4** 2081
[8] Nemov V V, Kasilov S V, Kernbichler W and Heyn M F 1999 *Phys. Plasmas* **6** 4622
[9] Mynic H E, Chu T K and Boozer A H 1982 *Phys. Rev. Lett.* **48** 322
[10] Mynic H E 1983 *Phys. Fluids* **26** 1008
[11] Shaing K C and Hokin S A 1983 *Phys. Fluids* **26** 2136
[12] Galeev A A and Sagdeev R Z 1973 *Voprosy Teorii Plazmy* vol 7 (Moscow: Atomizdat) p 205 (in Russian) (Engl. Transl. 1979 *Reviews of Plasma Physics* vol 7, ed M A Leontovich (New York: Consultants Bureau) p 257)
[13] Nührenberg J and Zille R 1988 *Phys. Lett.* A **129** 113
[14] Nemov V V 1999 *Phys. Plasmas* **6** 122